

Time required to injection-lock spin torque nanoscale oscillators

William Rippard, Matthew Pufall, and Anthony Kos

Citation: [Applied Physics Letters](#) **103**, 182403 (2013); doi: 10.1063/1.4821179

View online: <http://dx.doi.org/10.1063/1.4821179>

View Table of Contents: <http://scitation.aip.org/content/aip/journal/apl/103/18?ver=pdfcov>

Published by the [AIP Publishing](#)

Articles you may be interested in

[Phase locking of vortex-based spin-torque nanocontact oscillators by antivortices](#)

Appl. Phys. Lett. **102**, 052403 (2013); 10.1063/1.4790287

[Injection locking of tunnel junction oscillators to a microwave current](#)

Appl. Phys. Lett. **98**, 182503 (2011); 10.1063/1.3587575

[Injection locking of the gyrotropic vortex motion in a nanopillar](#)

Appl. Phys. Lett. **97**, 142503 (2010); 10.1063/1.3498009

[Phase-locking and frustration in an array of nonlinear spin-torque nano-oscillators](#)

Appl. Phys. Lett. **95**, 262505 (2009); 10.1063/1.3278602

[Modeling and experimental studies of magnetron injection locking](#)

J. Appl. Phys. **98**, 114903 (2005); 10.1063/1.2132513

The logo for AIP APL Photonics is displayed in a white font on a red background. The letters 'AIP' are large and bold, followed by a vertical bar and the words 'APL Photonics' in a smaller font.

APL Photonics is pleased to announce
Benjamin Eggleton as its Editor-in-Chief



Time required to injection-lock spin torque nanoscale oscillators

William Rippard, Matthew Pufall, and Anthony Kos

National Institute of Standards and Technology, 325 Broadway, Boulder, Colorado 80305, USA

(Received 29 January 2013; accepted 11 August 2013; published online 29 October 2013)

We have injection-locked a spin-transfer oscillator to a second-harmonic electrical input signal and measured the relative phase and amplitude of the device output as a function of DC current under steady-state conditions. The relative phase of the device varies quasi-linearly with DC bias, although the averaged amplitude decreases significantly outside of the spectrally determined locking range. By pulsing the injected microwaves, the time required for the device to phase-lock to the injected signal was measured as a function of microwave amplitude. The locking time varied quasi-linearly over the range of amplitudes studied, with the shortest locking times being a few nanoseconds. [<http://dx.doi.org/10.1063/1.4821179>]

Spin torque oscillators (STOs) have been injection locked to many impressed signals such as electrical currents,^{1–5} magnetic fields,^{6,7} and spin waves.^{8–11} STOs exhibit phase-coherence with the injection source, frequency-pulling, locking to harmonic and fractional signals, along with other phenomena similar to those observed in other non-linear oscillators. The ability of STO devices to lock to an impressed signal makes them attractive as potential nanoscale microwave devices. However, if the application requires a device to lock to either a time-varying (pulsed) or frequency-modulated signal, such as in network computing schemes,¹² it is not only important that the device lock to the impressed signal but that it also does so quickly. Here, we report measurements of the time required for a STO to become phase-coherent with an electrically injected second-harmonic microwave signal as a function of the impressed signal amplitude. Additionally, we present time-domain measurements of the device in the quasi-locked regime¹³ that show that, when locked, the STO maintains a well-defined relationship with the injected signal.

The device discussed here comprises a film stack of (bottom)SiO₂|Ta (3)|Cu(25)|Co₉₀Fe₁₀(10)|Cu(4.5)|Ni₈₀Fe₂₀(5)|Cu(3)|Ta(3) (all thicknesses in nanometers) with a nominal 65 nm diameter lithographically patterned electrical contact made to the top of the stack.¹⁴ In this pseudo-spin-valve, the NiFe layer acts as the free layer and the CoFe layer acts as the fixed layer. The data discussed here are taken in an applied field of 0.575 T applied approximately 10° away from the normal to the sample surface. Similar measurements of other devices in fields ranging from about 0.5 T to 0.7 T applied between 0° and 20° away from normal showed analogous behaviors to those presented here. Positive current values correspond to electrons flowing from the free layer into the fixed layer. All measurements were performed at room temperature.

Spectral-based injection-locking experiments are performed in a manner similar to that described elsewhere.^{3,16} The device is DC current-biased through the low frequency leg of a bias-tee to induce precession that is read out through the high-frequency leg of the bias-tee by a spectrum analyzer after amplification (55 db). A second microwave probe is brought into electrical contact with the top of the device and

is used to inject an additional microwave signal (either continuously or pulsed) at 20.96 GHz, approximately twice the fundamental frequency of the STO. The second harmonic signal was chosen so no significant parasitic at the STO oscillation frequency is present in the measured signal, which would complicate the analysis. The impedance mismatch between the 50 Ω microwave circuit and the device resistance $R_{\text{dev}} = 15 \Omega$ results in about half of the microwave voltage being reflected back to the source. The values reported for the injected root-mean-square microwave voltages seen by the device V_{RF} take this reflection and cabling losses into account.

Figure 1(a) shows the oscillation frequency of the STO, as determined by Lorentzian fits to the spectra, as a function of DC bias I_{DC} for several values of V_{RF} along with the raw spectra for no microwave drive (inset). For $V_{\text{RF}} = 0 \text{ V}$, the frequency of the device output varies roughly linearly with current. When V_{RF} is increased the device output changes, showing both frequency pulling to half the injection frequency and locking, the strengths of which depend on V_{RF} . The device is taken to be locked when its linewidth is equal to the 1 MHz resolution bandwidth of the spectrum analyzer (approximately 10% of its free-running linewidth), and the locking range is taken as the difference between the non-driven device oscillation frequencies at the minimum and maximum DC biases at which the device locks to the impressed signal. Fig. 1(b) shows the locking range as a function of V_{RF} . A linear fit gives the locking range going to 0 MHz at a $V_{\text{RF}} \approx 7 \text{ mV}$, roughly 5% of the DC voltage.

When locked, time-domain measurements can be used to determine the relative phase of the device as a function of DC bias. We first discuss the device behavior when the microwave signal is applied as a continuous-wave (CW). For these measurements, the microwave source is locked to a 10 MHz square-wave from a tabletop atomic clock in order to minimize long-term phase drift, and the device output is measured using a 13 GHz bandwidth (40 gigasamples per second) real-time storage oscilloscope that is triggered by the same 10 MHz signal. An 8 GHz to 11 GHz band-pass filter was added in front of the amplifier to ensure that it is not saturated by the impressed signal. The oscilloscope averages 4000 time traces of the device output. Any signal that is not

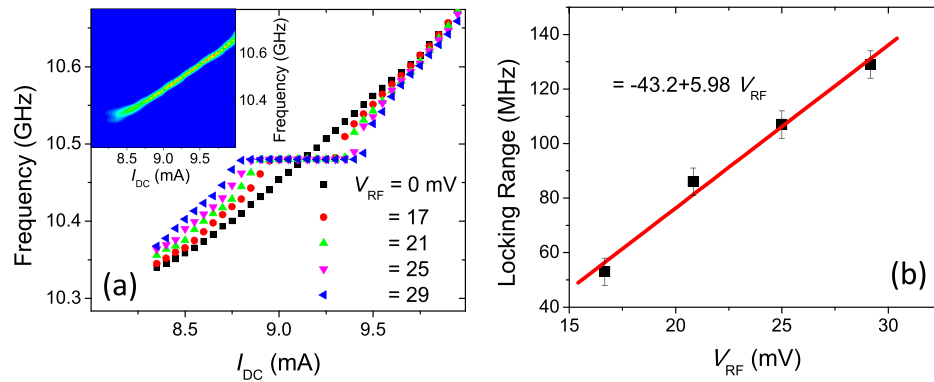


FIG. 1. (Inset) Two-dimensional plot showing the spectral output from the device on a logarithmic color scale (dark) $0.1 \mu\text{W}$ to (light) $6 \mu\text{W}$. The 55 dB amplifier gain is not divided out of the signal. (a) The oscillation frequency of the device as a function of DC bias for several values of V_{RF} . The error bars from Lorentzian fits to the spectra are smaller than the data points. (b) The locking range as a function of V_{RF} for 20.96 GHz. The result of a linear fit to the data is shown on the graph. The error bars are determined from the step size associated with I_{DC} and the linear dependence of the STO oscillation on DC bias.

phase-coherent with the 10 MHz trigger will average to ≈ 0 V during this process.

In the time traces shown below, we do not simply directly average the device output within the oscilloscope. Because the device is being locked to a second harmonic signal, it can identically lock to the impressed signal such that the device output is $\pm\pi$ out-of-phase with any previous time trace recorded during the averaging process. Hence, when the device is undergoing numerous phase-slips, such as in the quasi-locked regime, directly averaging traces will result in no net signal even though phase-locking occurs. The same problem is encountered in the pulsed measurements discussed below, because the device loses coherence between pulses. Even within the locking-range, the device goes through occasional $\pm\pi$ phase-slips so that direct signal averaging results in a waveform with an amplitude that varies with time (on the order of tens of seconds).

To circumvent this problem, instead of directly averaging the device output, the oscilloscope first takes the absolute value of the signal. This doubles the apparent frequency of the STO prior to performing the averaging, which makes it insensitive to $\pm\pi$ phase slips. We have experimentally verified that trigger jitter within the circuit smoothens the sharp cusps expected for the absolute value of a sine-wave, so that the averaging process results in an apparent sine wave as shown in the inset of Fig. 2(a) and below. All time-domain data shown here have been digitally high-pass filtered with a 5 GHz corner frequency that results in a signal centered about 0 V as opposed to an all-positive one. For the pulsed data discussed below, the filter serves to remove the low-frequency response of the capacitively coupled amplifier and does not significantly affect the data analysis.

We now turn our attention to the analysis of the time-domain data. For the data shown in the inset in Fig. 2(a), the frequency and amplitude of the microwave drive are kept fixed at 20.96 GHz and $V_{RF} = 21$ mV while the DC current bias through the device is varied. These data are then fit to a sine-wave having variable amplitude and phase, and a fixed frequency of 20.96 GHz. The resulting phase evolution of the device as function of DC current is shown in Fig. 2(a). The phase varies roughly linearly with current over much of the bias range, similar to Ref. 3, but saturates at the high biases. The larger value of the phase variation seen here as

compared to Ref. 3 results from the absolute-value function doubling the apparent frequency of the device, and hence doubling the fitted phase angle.

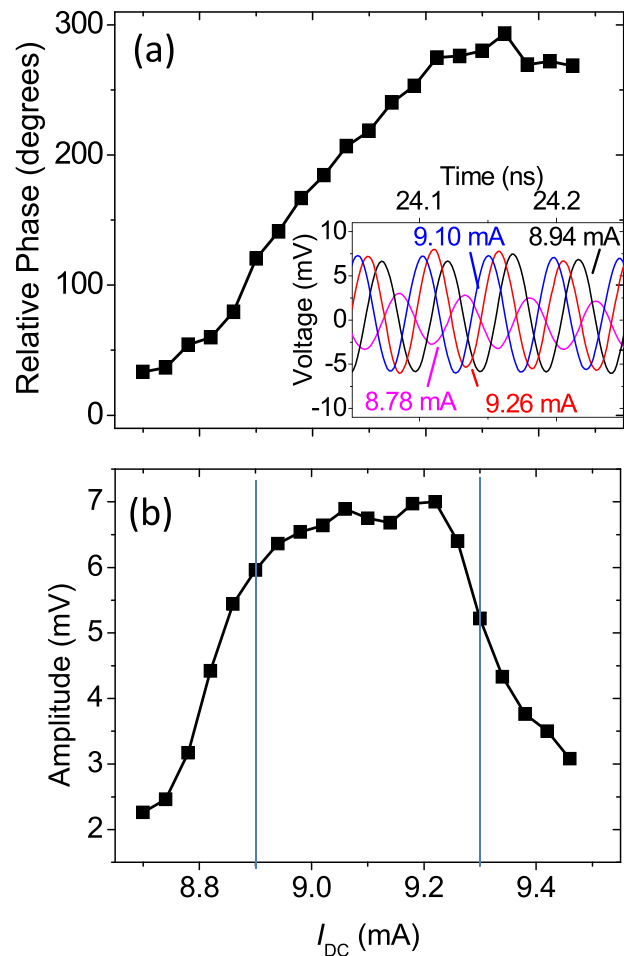


FIG. 2. (a) The relative phase variation of the device output for $V_{RF} = 21$ mV as a function of DC bias. The phase is determined by fitting a sine-wave having the amplitude and phase as fitting parameters while the frequency is fixed at 20.96 GHz over a fixed 10 ns interval of time. (Inset) shows small sections of the time-traces from which the phases and amplitudes of the device output were determined. (b) Plot of the fitted amplitude of the device output under the same conditions as in (a). The vertical lines are guides showing the locking range as determined by the spectral measurements of Fig. 1. For both (a) and (b), the error bars from the fits are smaller than the data points.

The amplitude of the fitted sine-wave is shown in Fig. 2(b) as a function of DC bias, along with vertical lines that show the locking range as determined by the spectral measurements. The averaged amplitude represents the fractional time that the device is phase-coherent with the impressed signal, although trigger jitter in the time-domain measurements will necessarily decrease the measured signal size as compared to the spectral ones. Between $I_{DC} = 8.9$ mA and 9.3 mA, the amplitude is roughly constant at approximately 6.8 mV, which is 75% of the value expected from the spectral measurements. This reduction is consistent with that observed when a microwave source is used to mimic the STO signal, and the same methodology is used to compare spectral and time-domain measurements, showing that the device is locked for a constant and large fraction of the measurement averaging time. Outside of this range, the averaged amplitudes decrease indicating the device is going through phase-slips even under CW conditions. However, as shown by the data in Fig. 2(a) even when the STO is outside of the spectrally determined locking range, it maintains a well-defined phase relationship with the impressed signal for the fraction of time that it is locked.

Above, we have largely reproduced our earlier results from a different device (Ref. 3), with the additions of improved time-domain measurements outside the spectrally determined locking range, a different method for detection and averaging of the real-time signals, and locking is done to a second-harmonic signal. These modifications were made so that we could unambiguously measure the time required for a device to lock to an impressed signal, which we focus on below. The same basic experimental setup is used as in the CW measurements with the exception that an additional custom low-jitter pulser, which is referenced to the same 10 MHz square wave, is added to the circuit to gate the microwave source. The pulser sends a 100 ns pulse to “turn on” the microwave source every 900 ns, creating a waveform with a 10% duty cycle, and a low-jitter trigger signal to the oscilloscope. The delay between microwave pulses allows the device to lose coherence with the previous pulse (the decoherence time of the free-running device was measured to be approximately 50 ns from time-domain measurements) before the next coherent microwave pulse arrives. The device output is

amplified, measured, and averaged as above for 4000 microwave pulses using the trigger from the pulser.¹⁵ Any signal that is not phase-coherent with the trigger from the pulser will average to ≈ 0 V during this process.

Figure 3(a) shows representative time traces for two different microwave pulse amplitudes (for $I_{DC} = 9.0$ mA) along with the envelope function of the microwave pulse itself. The turn-on of the impressed microwave pulse is relatively slow at 3 ns–4 ns, but it lacks any significant overshoot, the presence of which can complicate the locking-time analysis. Although the pulse begins to turn-on at time $t \approx 5$ ns, no measureable coherent signal from the device appears until $t \approx 10$ ns, well after the pulse amplitude has reached its maximum constant value. For later times, a clear signal can be measured for both values of V_{RF} (and those between them) and the amplitude of the device output grows, indicating that it is becoming more coherent with the impressed microwave signal.

The locking time is determined by first finding local maxima in the device output and fitting the resulting envelope with the expression $A(1 + \exp(-k(t - t_0)))^{-1}$, where A is an amplitude, k is an effective growth rate, and t_0 is a turn-on time. This expression, along with the fitted parameters, is then used to determine the time that the device output reaches 90% of its average final amplitude. We chose to compare that time to the time V_{RF} reaches 90% of its amplitude, which does not significantly change with the values of V_{RF} , in order to define the locking time t_{lock} (Fig. 3(b)). The data show that t_{lock} depends quasi-linearly on V_{RF} over the range studied here. Given the relatively small range of V_{RF} over which the locking time was measured, this is consistent with the model of Adler that predicts the locking time should be inversely proportional to the normalized drive (i.e., $(V_{RF}/V_{DC})^{-1}$).^{16,17} While the measured locking times are similar to those predicted in Ref. 17 for similar values of normalized drive, the saturation of t_{lock} with V_{RF} predicted therein is not observed. This discrepancy may result from having a slightly different applied field strength and geometry, the device being locked to a second harmonic signal, which change the nonlinearities in the device and affect locking behavior,⁷ and thermal effects, or a combination thereof.

The data show that the device can take as little as a few nanoseconds to lock to the impressed signal, i.e., within a

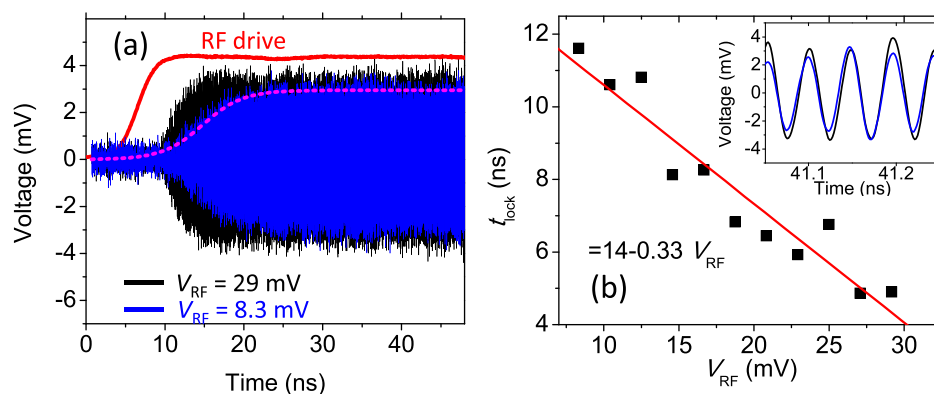


FIG. 3. (a) Plot of the averaged device output for two values of V_{RF} for $I_{DC} = 9.0$ mA as a function of time, along with the envelope function for the injected microwave voltage (shown on an arbitrary voltage scale) that serves only as a time reference. The magenta curve (dashed line) is the fit of the envelope of the $V_{RF} = 8.3$ mV time trace. (b) The value of t_{lock} as a function of V_{RF} along with a linear fit. The error bars for t_{lock} as determined from the fits are smaller than the data points. (Inset) Plot of partial time-traces from the data shown in (a) demonstrating the phase-coherence of the device output. The colors correspond to those in (a).

few tens of precessional cycles of the magnetization, and within times that are significantly less than its decoherence time. For much larger or smaller values of V_{RF} than those shown here, this linear dependence must change since a finite value for t_{lock} is expected even for the largest values of V_{RF} and a finite microwave signal must be present in order for locking to occur. For completeness, we show part of the time-traces in Fig. 3(a) in the inset of (b) demonstrating phase-coherent signals from the device.

Choosing other uniform threshold values does not qualitatively change the data shown in Fig. 3(b). However, if a lower threshold value is chosen for only the impressed signal (e.g., the time required for the pulse to reach the ≈ 7 mV level required for CW locking) a few nanoseconds would be added to the time axis. We note that the differences in the amplitudes of the device output shown in Figs. 2(b) and 3(a) largely result from the additional ≈ 5 ps trigger jitter from the pulser, as opposed to only partial locking of the device. For V_{RF} less than ≈ 8 mV the amplitudes and uniformity of the waveforms in the pulsed experiments are significantly degraded, which is consistent with the locking range determined in the CW measurements discussed above.

In summary, we have measured the time required to injection lock a STO to a second-harmonic signal as a function of V_{RF} and found that, over the range of drives studied here, the locking time varies roughly linearly with drive amplitude, which is consistent with the theory of Adler. However, this functional form should change for much larger or smaller drive voltages. For a strong enough drive, the locking time can be a little as a few nanoseconds, showing that the devices are relatively frequency agile. These measurements have significant implications for potential applications in which STO devices are locked to a time-varying signal, and allow for more quantitative comparison with theory.

We thank S. Levitan and G. Bourianoff for suggesting this course of research, and S. Russek, R. Goldfarb, and E. Evarts for helpful commentary on the preparation of this manuscript.

- ¹M. Quinsat, J. F. Sierra, I. Firastrau, V. Tiberkevich, A. Slavin, D. Gusakova, L. D. Buda-Prejbeanu, M. Zarudniev, J.-P. Michel, U. Ebels, B. Dieny, M.-C. Cyrille, J. A. Katine, D. Mauri, and A. Zeltser, *Appl. Phys. Lett.* **98**, 182503 (2011).
- ²M. d' Aquino, C. Serpico, R. Bonin, G. Bertotti, and I. Mayergoz, *Phys. Rev. B* **82**, 064415 (2010).
- ³W. Rippard, M. Pufall, S. Kaka, T. Silva, S. Russek, and J. Katine, *Phys. Rev. Lett.* **95**, 067203 (2005).
- ⁴A. Dussaux, A. V. Khvalkovskiy, J. Grollier, V. Cros, A. Fukushima, M. Konoto, H. Kubota, K. Yakushiji, S. Yuasa, K. Ando, and A. Fert, *Appl. Phys. Lett.* **98**, 132506 (2011).
- ⁵B. Georges, J. Grollier, M. Darques, V. Cros, C. Deranlot, B. Marcilhac, G. Faini, and A. Fert, *Phys. Rev. Lett.* **101**, 017201 (2008).
- ⁶P. Tabor, V. Tiberkevich, A. Slavin, and S. Urazhdin, *Phys. Rev. B* **82**, 020407 (2010).
- ⁷S. Urazhdin, P. Tabor, V. Tiberkevich, and A. Slavin, *Phys. Rev. Lett.* **105**, 104101 (2010).
- ⁸S. Kaka, M. R. Pufall, W. H. Rippard, T. J. Silva, S. E. Russek, and J. A. Katine, *Nature* **437**, 389–392 (2005).
- ⁹F. B. Mancoff, N. D. Rizzo, B. N. Engel, and S. Tehrani, *Nature* **437**, 393–395 (2005).
- ¹⁰A. Ruotolo, V. Cros, B. Georges, A. Dussaux, J. Grollier, C. Deranlot, R. Guillemet, K. Bouzehouane, S. Fusil, and A. Fert, *Nat. Nanotechnol.* **4**, 528–532 (2009).
- ¹¹Y. Pogoryelov, P. K. Muduli, S. Bonetti, E. Iacocca, F. Mancoff, and J. Åkerman, *Appl. Phys. Lett.* **98**, 192501 (2011).
- ¹²F. Macià, A. D. Kent, and F. C. Hoppensteadt, *Nanotechnology* **22**, 095301 (2011).
- ¹³B. Razavi, *IEEE J. Solid-State Circuits* **39**, 1415 (2004).
- ¹⁴W. Rippard, M. Pufall, S. Kaka, S. Russek, and T. Silva, *Phys. Rev. Lett.* **92**, 027201 (2004).
- ¹⁵See supplementary material at <http://dx.doi.org/10.1063/1.4821179> for a schematic of the measurement set-up and a brief description.
- ¹⁶R. Adler, *Proc. IRE* **34**, 351 (1946).
- ¹⁷Y. Zhou, V. Tiberkevich, G. Consolo, E. Iacocca, B. Azzarboni, A. Slavin, and J. Åkerman, *Phys. Rev. B* **82**, 012408 (2010).